Reinforcement of Polypropylene Using Sisal Fibers Grafted with Poly(methyl methacrylate)

X. P. Zhou,[1,2] R. K. Y. Li,[1] X. L. Xie,[2] S. C. Tjong[1]

[1]*Department of Physics and Materials Science, City University of Hong Kong, Tat Chee Avenue, Kowloon, Hong Kong, China*
[2]*Department of Chemistry, Huazhong University of Science and Technology, Wuhan, China*

Received 24 January 2002; accepted 16 April 2002

ABSTRACT: Sisal fiber (SF) surface modification was carried out by grafting with methyl methacrylate (MMA) using cerium and ammonium nitrate as initiator. The effects of reaction time, monomer, and initiator concentration on the grafting parameters were systematically investigated. The results showed that MMA was successfully grafted onto the sisal fiber surface. The PMMA-grafted sisal fibers were melt blended with polypropylene (PP) and then injection molded. The PP/SF composites were characterized by means of thermal analysis, mechanical testing, wide-angle X-ray diffraction, and SEM examination. PMMA grafted onto the surface of SF enhanced the intermolecular interaction between the reinforcing SF and PP matrix, improved the dispersion of SF in the PP matrix, and promoted the formation of β-crystalline PP. These enhanced the thermal stability and mechanical properties of PP/SF composites. © 2003 Wiley Periodicals, Inc. J Appl Polym Sci 88: 1055–1064, 2003

Key words: polypropylene; composites; mechanical properties; modification; graft copolymers

INTRODUCTION

Sisal fiber (SF)–reinforced thermoplastic polymer–matrix composites have attracted considerable attention. The low cost, good specific properties, and environmental friendliness of sisal fibers, and the possibility of injection molding[1–5] are possible reasons for the popularity. Comprehensive reviews on natural fiber–reinforced composites have been given in reports by Bledzki and Gassan,[6] Saheb and Jog,[7] and Li et al.[8] Recently, Xie and coworkers[9] prepared polypropylene (PP)/SF composites by melt-mixing and injection molding. However, the poor interfacial bonding affected the reinforcement of SF to the PP matrix. The approaches used to improve the interfacial characteristic between SF and polymer matrices including chemical treatment, heat treatment, coupling agent coating, and γ-irradiation on the sisal fiber surface as well as adding compatibilizer such as maleic–anhydride-grafted-SEBS.[1–3,10–17] The surface modification of fillers by grafting polymerization using organic monomers has been found to be an effective method to improve the interfacial bonding between filler and polymer matrix. Xie and coworkers[18] reported that the *in situ* polymerization of methyl methacrylate (MMA) onto the surface of talc remarkably improved the mechanical properties of poly(vinyl chloride) (PVC)/talc composites. Canché-Escamilla and coworkers[19,20] reported that the grafting polymerization of MMA onto henequen cellulose fibers enhanced the interfacial adhesion between the henequen fiber and the PVC matrix.

In this work, the surface of sisal fibers was modified by grafting polymerization using MMA. The treated SF was subsequently used to fill PP. It is expected that the PMMA grafted onto the surface of SF can improve the mechanical properties of the resulting PP–matrix composites.

EXPERIMENTAL

Materials

The PP homopolymer (Grade T30S; melt flow rate of 4 g/10 min) used in this work was supplied by Wuhan Petrochemical Co. (China). The sisal fibers (SF) were obtained from Guangxi Sisal Fiber Co. (China). They were chopped into pieces approximately 8 mm long. Reagent-grade MMA from Shanghai Chemical Co. (China) was purified by distillation under reduced pressure to remove the inhibitor. Cerium and ammonium nitrate (CAN) was used as initiator. The water used was distilled and deionized.

Alkali treatment of sisal fiber

The chopped sisal fibers and a 10% solution of NaOH were put into a stainless steel vessel that was kept at

Correspondence to: R. Li (aprkyl@cityu.edu.hk).
Contract grant sponsor: Research Grants Council of the Hong Kong Special Administrative Region, China; contract grant number: 9040422.

25°C and stirred for 1 h. Afterward, the sisal fibers were washed thoroughly with water to remove any excess NaOH, after which they were dried under vacuum. The effects of alkali treatment on sisal fibers was discussed in a number of previous studies.[2,4]

Grafting polymerization procedures

The grafting polymerization of MMA onto SF surfaces was carried out using the procedures as previously employed by Canché-Escamilla et al.[19] Sisal fibers were dried and weighed (W_{SF}) before being mixed with water (1 : 1 weight ratio) in a 1-L glass flask that had been immersed in a constant temperature bath at 30°C. After removing all the oxygen, nitrogen was sparged for 1 h. Afterward, different percentages of MMA monomers and initiator (CAN dissolved in 1*N* nitric acid) were added to start the reaction. After the reaction was ended, the treated sisal fibers were washed with water and then dried to constant weight ($W_{Product}$) in a vacuum oven at 60°C. $W_{Product}$ in eq. (1) is the total weight of sisal fiber, PMMA grafted onto the SF surfaces, and PMMA just deposited but not grafted onto the fiber surface. The percentage of conversion of the MMA monomers was determined by the following equation:

$$\text{Percentage of MMA conversion} = \left(\frac{W_{Product} - W_{SF}}{\text{weight of monomer used}}\right) \times 100\% \quad (1)$$

Percentage of PMMA grafting

To remove the ungrafted PMMA from the sisal fiber surface, the sisal fibers after grafting polymerization were immersed in acetone for 24 h in a Soxhlet apparatus, and dried under vacuum to a constant weight ($W_{PMMA\text{-}g\text{-}SF}$). The percentage of PMMA grafted onto the SF surface was calculated by the following equation:

$$\text{Percentage of PMMA grafting} = \left(\frac{W_{PMMA\text{-}g\text{-}SF} - W_{SF}}{W_{SF}}\right) \times 100\% \quad (2)$$

where W_{SF} is the weight of SF before the grafting reaction [the same W_{SF} as in eq. (1)].

FTIR spectroscopy was applied to characterize the changes in the chemical structure of SF after grafting polymerization. Thin-film specimens were pressed with KBr powder.

Preparation of reinforced PP composites

Untreated sisal fiber (U-SF), alkali-treated sisal fiber (AT-SF), and PMMA-grafted sisal fiber (PMMA-*g*-SF) were used, respectively, to prepare PP matrix composites. The melt blending of the sisal fibers with PP were conducted using a two-roll mill operated at 175°C for 10 min. Fiber contents for all the composites were kept at 20 wt %. The melt-blended composites were injection molded into tensile bars and Izod impact specimens. The injection barrel temperatures were set at 185, 187, and 187°C.

Thermal analysis

The thermal degradation characteristics of the PP/SF composites were carried out using a Seiko thermogravimetric analyzer (model SSC/5200; Seiko Instruments, Tokyo, Japan). The weight loss against temperature was measured at a heating rate of 10°C/min in helium atmosphere from 50 to 500°C.

DSC measurements were conducted using a Perkin–Elmer DSC-7 instrument (Perkin Elmer Cetus Instruments, Norwalk, CT) at a heating rate of 10°C/min under dry nitrogen atmosphere. Before the DSC recording, all samples were heated to 220°C and kept at this temperature for 3 min before being quenched to ambient temperature, to eliminate the influence of any previous thermal histories. For nonisothermal crystallization measurements, the samples were heated to and kept at 220°C for 3 min, and then cooled at a cooling rate of 10°C/min.

Morphology observations

Fracture surface morphologies of the composites were observed in a scanning electron microscope (SEM, model JEOL JSM 820; JEOL, Peabody, MA). All fractured surfaces were coated with a thin layer of gold before SEM examination.

Wide-angle X-ray diffraction measurements

Wide-angle X-ray diffraction (WAXD) patterns of the composite samples were taken with a diffractometer (Philips model X'Pert; The Netherlands). The operating conditions were: Cu–K_α radiation with a Ni filter, voltage 40 kV, current 50 mA, divergence slit 1°, receiving slit 0.3 mm, and scattering slit 1°. The angular scale and recorder reading (2θ) were calibrated to an accuracy of $\pm 0.01°$. Scans in the reflection mode were performed within the 2θ range of 5 to 40°.

Mechanical properties

The tensile behavior was determined using an Instron tensile tester (model 4206) at room temperature under a crosshead speed of 1 mm/min. The Izod impact test was conducted using a Ceast pendulum impact tester (Ceast, Italy).

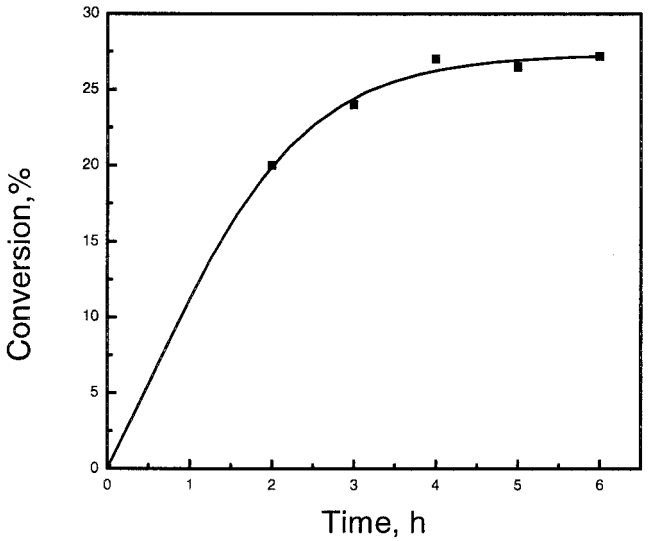

Figure 1 Reaction kinetic curve for the grafting polymerization of PMMA onto SF.

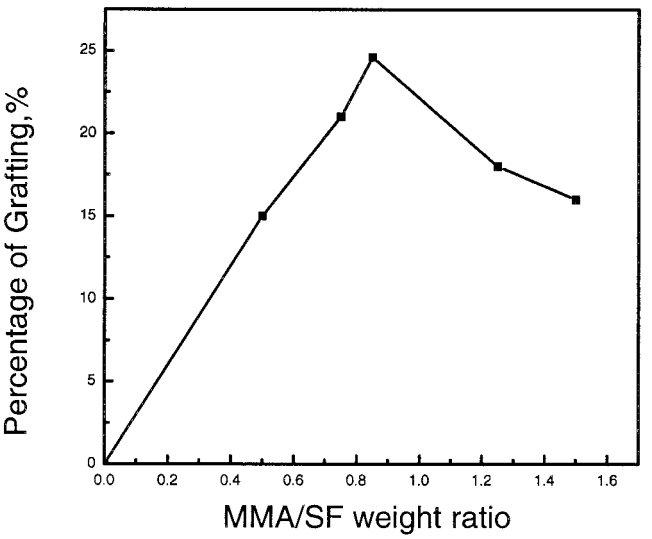

Figure 2 Percentage of grafting as a function of MMA/SF ratio. The initiator is 6 m*M* CAN and the reaction time is 4 h.

Dynamic mechanical analysis

Dynamic mechanical analysis (DMA) was conducted with a TA Instruments dynamic mechanical analyzer (model 2980; TA Instruments, New Castle, DE) at a fixed frequency of 10 Hz and oscillation amplitude of 0.15 mm. The temperature range studied was from −40 to 120°C with a heating rate of 2°C/min.

RESULTS AND DISCUSSION

Kinetics for the grafting polymerization of PMMA onto SF

Figure 1 shows the reaction kinetics of the grafting polymerization of PMMA onto SF, with a 1 : 1 weight ratio of MMA to SF, and the concentration of CAN was 6 m*M*. The results indicated that the polymerization conversion of MMA increased rapidly at the beginning of polymerization. With further increases of reaction time, the conversion of MMA was increased only slightly. After 4 h, the conversion reached an equilibrium value (~ 27%). The behavior is the same as the general free-radical polymerization.

Figure 2 shows the effect of MMA/SF weight ratio on the percentage of PMMA grafting. We can see that there is a maximum percentage of PMMA grafting when the MMA/SF weight ratio is about 0.9. Figure 3 shows the effect of initiator concentration on the percentage of PMMA grafting. It can be seen that the percentage of grafting increased with increasing CAN concentration up to 8 m*M*. This is because the flux of free radicals increased with increasing initiator concentration, which enhanced the possibility of initiating reactive sites on the SF where PMMA can be grafted. However, when the initiator concentration was greater than 8 m*M*, the homopolymerization of the relatively water-soluble MMA became important as a consequence of the high concentration of Ce(IV) ions in the aqueous phase. These reactions should retard the grafting reaction. These are in accordance with the results reported by Canché-Escamilla et al.[19].

Characterization of the PMMA-grafted sisal fibers

Figure 4 compares the FTIR spectra of the U-SF and PMMA-*g*-SF. The PMMA-grafted sisal fibers were extracted by acetone to remove the PMMA molecules that were just deposited but not grafted firmly onto the sisal fibers. It can be seen that there is an absorption peak located at about 1730 cm^{-1} for the PMMA-

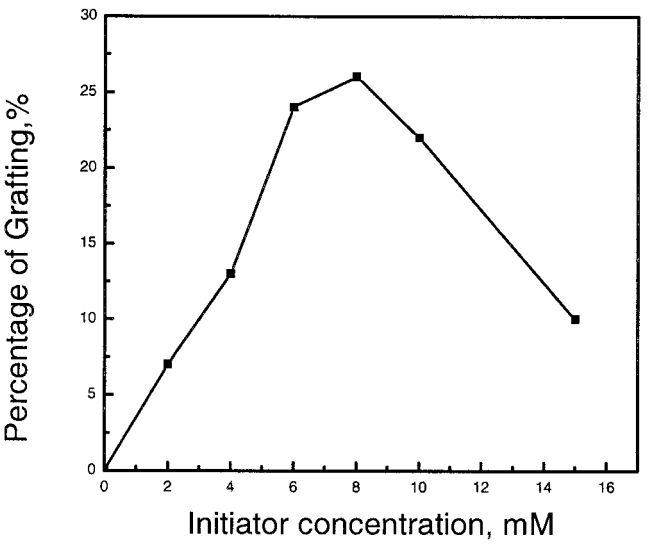

Figure 3 Effect of initiator concentration on the percentage of grafting of PMMA onto SF. The MMA/SF ratio used is 1 : 1 and the reaction time is 4 h.

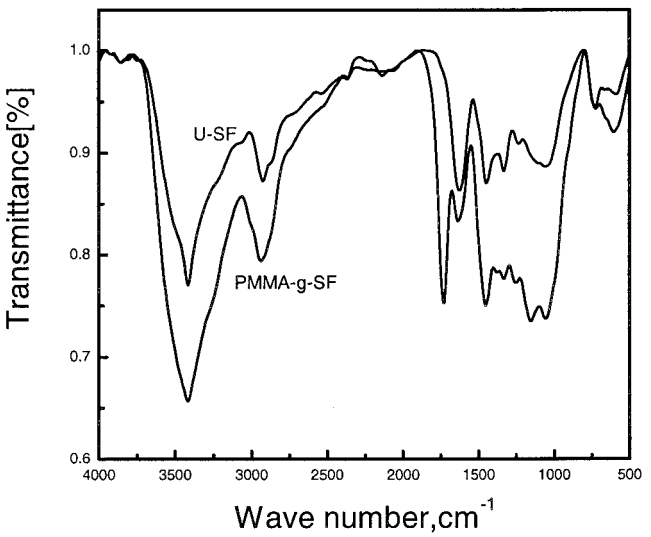

Figure 4 FTIR spectra of untreated and PMMA-grafted sisal fiber.

grafted SF. The peak is associated with the stretching vibration of the carbonyl groups of PMMA. This shows that PMMA had been successfully grafted onto the sisal fiber surfaces.

SEM micrographs of the surfaces of U-SF and PMMA-*g*-SF are shown in Figure 5(a) and (b), respectively. It can be seen that the grafting polymerization of PMMA onto the surface of SF led to microfiber fibrillation (i.e., breaking down of the fiber bundles into small fibers). This could have increased the effective surface area available for contact with the matrix in the composite, as well as reduced the diameter of sisal fibers, thereby increasing their aspect ratio. Moreover, there was a PMMA layer covering the surface of SF. The improvement in wettability property and increase in aspect ratio may offer better fiber–matrix interface adhesion and improve stress transfer. These will give rise to improvement in mechanical properties.

Figure 6 shows the thermal gravimetric (TG) and the derivative of the TG (DTG) curves for the untreated (U-SF), NaOH-treated (AT-SF), and PMMA-grafted (PMMA-*g*-SF) sisal fibers. From these curves, the 5% weight loss temperature ($T_{5\%}$) and maximum weight loss temperature ($T_{\max}$, which is defined as the peak on the DTG curve) can be obtained and are listed in Table I. Also listed in Table I are the weight losses at 100°C and $T_{\max}$ (which are designated as W_{100} and $W_{T\max}$, respectively). From the TG curve of the untreated SF, it can be seen that the weight loss attributed to the evaporation of the absorbed moisture below 100°C is more substantial than the alkali-treated or PMMA-grafted sisal fibers. There are two maximum peaks in the DTG curve for the untreated sisal fiber [Fig. 6(b)], which are related to the decomposition of the organic gum and cellulose fiber, respectively. However, for both alkali-treated and PMMA-grafted sisal fibers, only one peak can be identified. This is because the alkali treatment and grafting polymerization remove the organic gums in sisal fibers. Therefore, only the peak for the decomposition of the cellulose can be detected. Because the organic gums have a tendency to absorb moisture, its removal in both the alkali-treated and PMMA-grafted sisal fibers led to an increase in $T_{5\%}$ of these treated sisal fibers. It is worth noting that the 5% weight loss temperature ($T_{5\%}$) of PMMA-grafted sisal fiber is higher than that of either untreated or alkali-treated sisal fibers. At the same time, the W_{100} and $W_{T\max}$ of PMMA-grafted SF are less than those of untreated and alkali-treated sisal fibers. These results demonstrate that the presence of the grafted PMMA enhances the thermal stability of sisal fiber.

Thermal properties of PP/SF composites

The TG and DTG curves for the PP/SF composites are shown in Figure 7(a) and (b), respectively. It can be seen that there are two maximum peaks in the DTG curves (temperatures for these two peaks are designated $T_{\max SF}$ and $T_{\max PP}$), which are related to the thermal decomposition of SF and PP, respectively, in

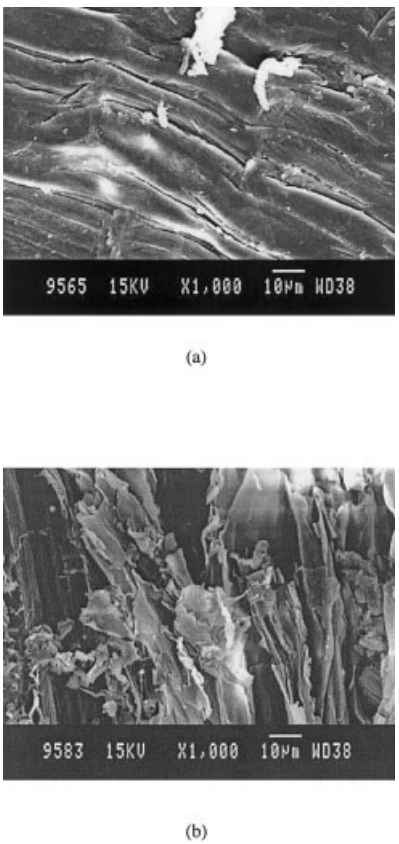

Figure 5 SEM micrographs of (a) untreated sisal fiber and (b) PMMA-grafted sisal fiber.

the PP/SF composites. $T_{5\%}$, T_{maxSF}, T_{maxPP}, and the weight loss at T_{maxSF} and T_{maxPP} (W_1 and W_2) of PP and the different PP/SF composites were determined and are listed in Table II.

Apparently, $T_{5\%}$ and T_{maxPP} for the PP/PMMA-*g*-SF composite are higher than those of PP/U-SF and PP/AT-SF composites, and the W_1 and W_2 of the PP/PMMA-*g*-SF composite are less than those of PP/U-SF and PP/AT-SF composites. These results indicate that the thermal stability of PP/SF composites is improved by grafting the sisal fiber surface with PMMA. This may be because grafting of the PMMA molecules enhances the intermolecular interaction between PP and SF, and hence improves their interfacial adhesion.

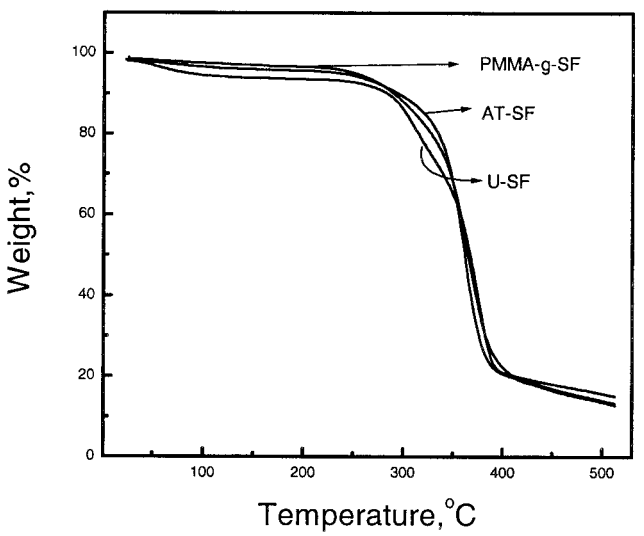

(a)

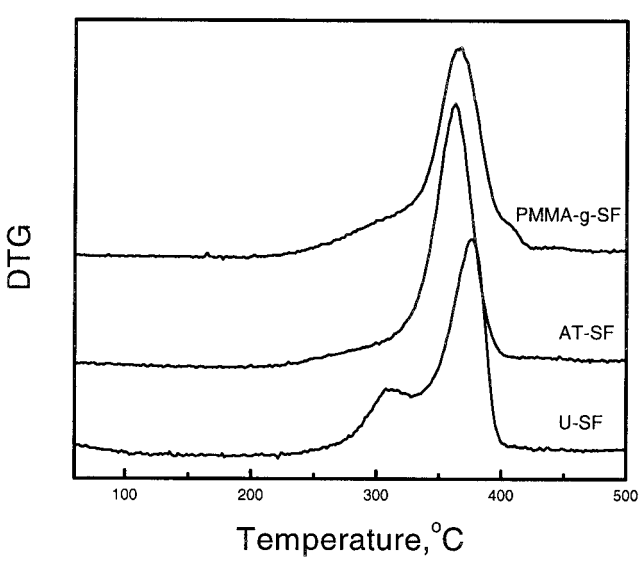

(b)

Figure 6 TGA results for the sisal fibers: (a) TG curves; (b) DTG curves.

TABLE I
Thermogravimetric Properties of the Different Pretreated Sisal Fibers

Sample	W_{100} (%)	$T_{5\%}$ (°C)	T_{max} (°C)	W_{Tmax} (%)
PMMA-grafted SF	2.3	253	367	49.8
NaOH-treated SF	3.4	237	364	54.0
Untreated SF	5.5	85	305/373	60.0

The DSC heating and cooling thermograms for the PP/SF composites are shown in Figure 8(a) and (b), respectively. The onset and peak melting temperature (T_m and T_{mp}, respectively), crystallization temperature (T_c), and heat of fusion (ΔH_m) for the PP phase in the PP/SF composites were determined from the DSC thermograms and are listed in Table III. It can be seen that T_m values of the PP phase in the three types of composites are about the same, but T_{mp} and T_c are remarkably reduced in the PP/PMMA-*g*-SF composite compared with those in the PP/U-SF and PP/AT-SF composites.

It is generally known that the degree of supercooling ΔT, which is defined as the difference between T_{mp} and T_c, can be used to characterize the crystallization behavior of polymer melts. A decrease in ΔT generally indicates that the crystallization rate of the polymer is accelerated. The ΔT values of the PP/SF composites investigated are listed in Table III. Apparently, the crystallization rate of the PP phase in the PP/PMMA-*g*-SF composite is slower than those of the PP/U-SF and PP/AT-SF composites.

The degree of crystallinity (X_c) of the PP/SF composites can be determined from their heat of fusion normalized to that of PP according to the following equation:

$$X_c = \frac{\Delta H_m}{\Delta H^*} \times 100\% \quad (3)$$

where ΔH_m is the melting heat of the PP/SF composite normalized to that of PP and ΔH^* is the melting heat of PP with 100% crystallinity. In applying eq. (3), the value of ΔH^* as obtained from the literature[21] for 100% crystalline PP is 240.5 J/g. The X_c values for the PP/SF composites as calculated from eq. (3) are also tabulated in Table III. It can be seen that X_c of the PP/PMMA-*g*-SF composite is lower than that of either the PP/U-SF or the PP/AT-SF composite.

In our previous study,[9] it was found that sisal fibers act as nucleation sites for PP spherulites, and hence accelerate the crystallization rate and enhance the de-

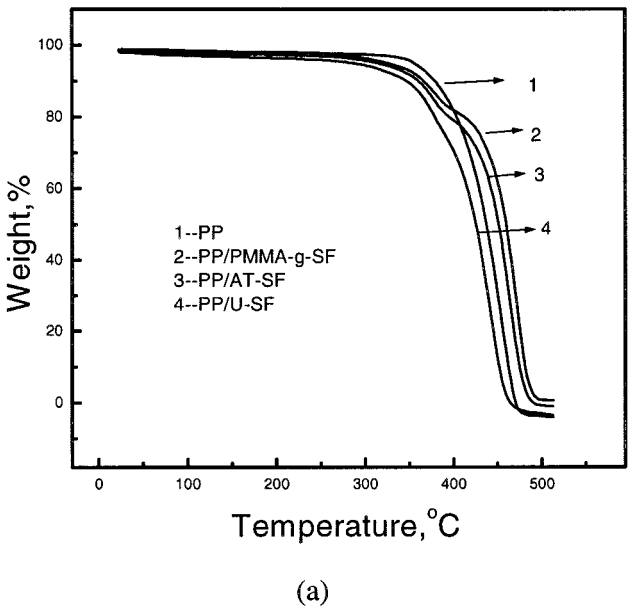

(a)

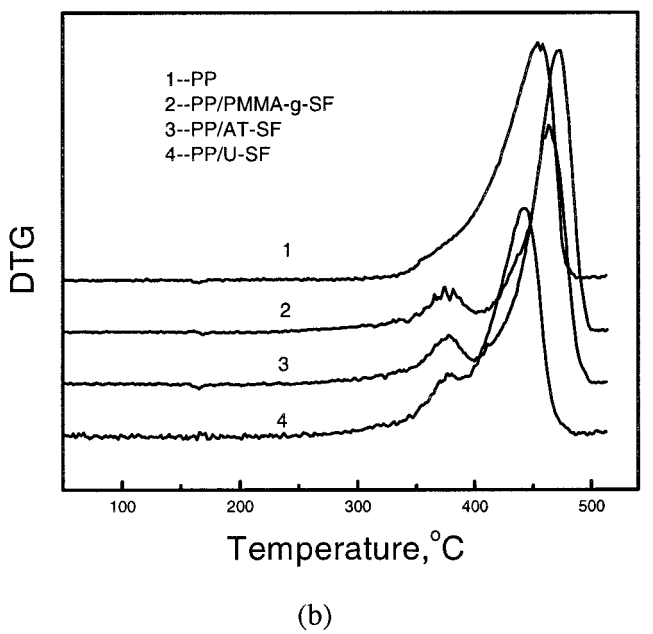

(b)

Figure 7 TGA results for the PP/SF composites: (a) TG curves; (b) DTG curves.

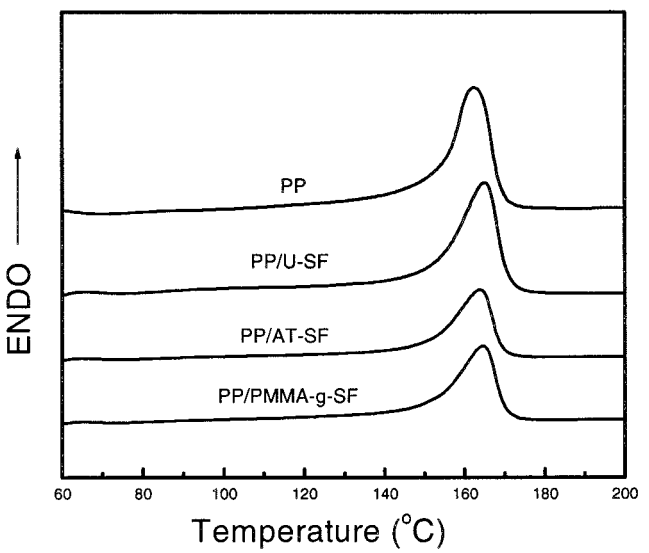

(a)

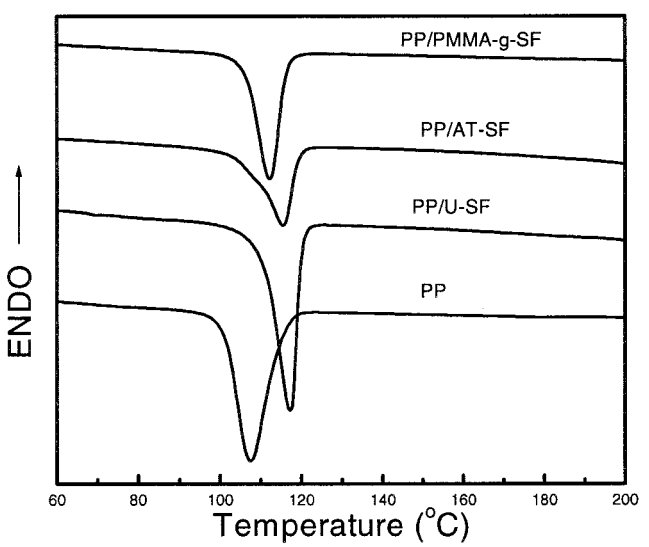

(b)

Figure 8 DSC measurements for PP and the different PP/SF composites: (a) heating scans; (b) cooling scans.

TABLE II
Thermogravimetric Properties of PP/SF Composites

Sample	$T_{5\%}$ (°C)	T_{maxSF} (°C)	W_1 (%)	T_{maxPP} (°C)	W_2 (%)
PP/PMMA-*g*-SF	325.3	373.4	13.7	470.6	69.0
PP/AT-SF	286.0	376.8	14.6	463.1	70.0
PP/U-SF	283.3	376.0	18.6	444.4	78.2

gree of crystallinity of PP. As discussed earlier in this study, the PMMA grafted onto the surface SF enhanced the intermolecular interaction between PP and SF, and hence hindered the crystallization of the PP phase in the PP/PMMA-*g*-SF composite.

In measurements of the thermal properties, very small sample sizes were used. However, it was observed that the sisal fibers were in general dispersed uniformly in the PP matrix. The thermal analysis results are therefore quite reproducible.

TABLE III
Melting and Crystallization Properties of the PP Phase in PP/SF Composites

Sample	T_m (°C)	T_{mp} (°C)	T_c (°C)	T_{cp} (°C)	ΔT (°C)	ΔH (J/g)[a]	X_c (%)
PP/U-SF	152.0	164.8	120.0	117.2	44.8	97.88	40.7
PP/AT-SF	150.9	163.7	119.4	115.7	44.3	92.29	38.4
PP/PMMA-*g*-SF	152.0	162.4	116.4	112.1	46.0	88.37	36.7

[a] Corrected for per gram of PP in the composites.

Dynamic mechanical properties of PP/SF composites

The dynamic mechanical properties of PP homopolymer and the PP/SF composites are shown in Figure 9. From these curves, selected values of storage modulus (E') and loss factor (tan δ) were obtained and are listed in Table IV. The evolution of E' with temperature for the different systems is shown in Figure 9(a). Over the whole temperature range of measurement, the following order is revealed:

$$E'_{\text{PP/PMMA-}g\text{-SF}} > E'_{\text{PP/AT-SF}} > E'_{\text{PP/U-SF}} > E'_{\text{PP}}$$

Figure 9(b) shows the evolution of tan δ with temperature. From the plots, the tan δ peak for PP homopolymer is measured to be 17.5°C, whereas for all the sisal fiber–reinforced composites, the peaks were located at about 15°C. The peak is correlated to the β-relaxation of PP and corresponds to the glass transition of the amorphous domains.[22] This maximum peak is assigned as the glass-transition temperature (T_g). The experimental results prove that the T_g occurs at lower temperature in the PP/SF composites. This phenomenon was also observed in PP/talc composites.[23] The decrease of T_g in the PP/SF composites can be explained with the aid of DSC results. The sisal fibers act as nucleating sites in PP/SF composites, which lead to faster crystallization of PP, as discussed earlier. This crystallization speedup causes an amorphous phase with higher mobility in the composites, which results in a lower T_g value.

In the insert in Figure 9(b), the different tan δ curves are separated for easy inspection. It can be seen that there is an additional tan δ peak at about 90°C in the PP/PMMA-*g*-SF composite but not in the other samples. The peak is the T_g of the PMMA fragments that grafted onto the surface of SF.

Values of tan δ at T_g for the PP phase in the different composites and PP homopolymer are listed in Table IV. It is obvious that the intensity of the transition decreases when SF is incorporated into the PP matrix. The surface modification of SF has a considerable effect on the tan δ intensity of the PP phase in the composites. At the glass-transition temperature, the magnitude of tan δ reveals the following order:

$$(\tan\delta)_{\text{PP}} > (\tan\delta)_{\text{PP/PMMA-}g\text{-SF}} > (\tan\delta)_{\text{PP/AT-SF}} > (\tan\delta)_{\text{PP/U-SF}}$$

In polymers, the loss factor (tan δ) is generally attributed to the amorphous phase and can be given by the following equation[24]:

$$\tan\delta \approx (1 - X_c) \times (\tan\delta)_a \quad (4)$$

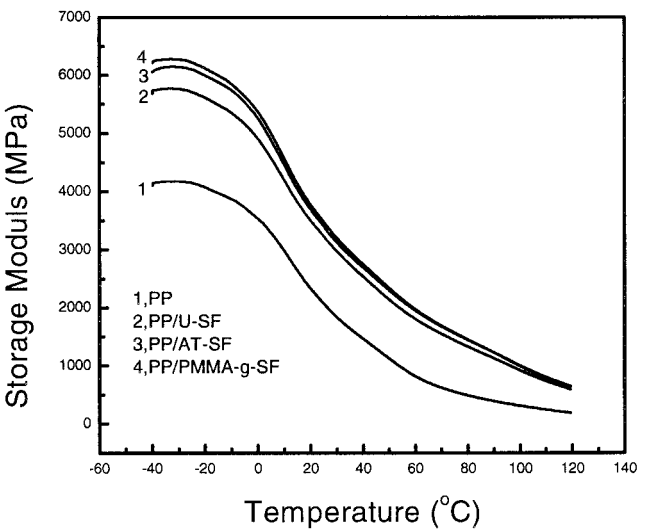

(a)

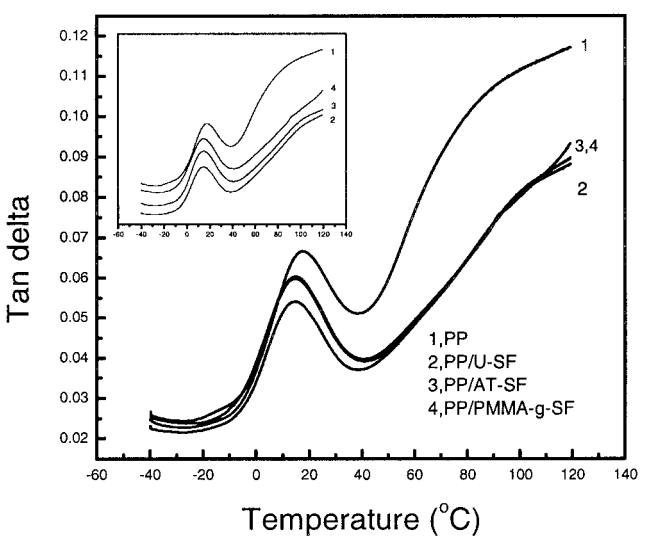

(b)

Figure 9 DMA measurements for PP and the different PP/SF composites: (a) storage modulus (E'); (b) tan δ.

TABLE IV
Dynamic Mechanical Properties of PP and the Different PP/SF Composites

Sample	E' (GPa)		tan δ ($\times 10^{-2}$)		T_g (°C)	tan δ at T_g ($\times 10^{-2}$)
	−20°C	30°C	−20°C	30°C		
PP	4.1	1.8	2.54	5.55	17.5	6.67
PP/U-SF	5.6	3.0	2.42	4.05	14.5	5.41
PP/AT-SF	6.0	3.1	2.35	4.46	14.7	5.98
PP/PMMA-*g*-SF	6.1	3.2	2.22	4.49	14.9	6.03

where X_c is the degree of crystallinity and the subscript *a* refers to the contribution of the amorphous phase. Equation (4) shows that the intensity decreases with the increasing degree of crystallinity. By comparing the tan δ values at T_g listed in Table IV and the crystallinity (X_c listed in Table III) for the different composites, our results are in accordance with eq. (4).

Morphology of PP/SF composites

Figure 10 shows the impact-fractured surfaces for the PP/U-SF, PP/AT-SF, and PP/PMMA-*g*-SF composites. For the PP/U-SF composite, adhesion between the PP matrix and the untreated SF is poor. During crack growth, the untreated SF was pulled out from the PP matrix, and the surface of the fiber pull-out site was very smooth [Fig. 10(a)]. After SF was treated by NaOH, the interfacial bonding in PP/AT-SF composite was improved, and the surface of the fiber pull-out site was more rough [Fig. 10(b)]. The sisal fiber surface adhesive characteristics were improved in NaOH treatment by removing natural and artificial impurities, thereby producing a rough surface topography.[2,10] For the PP/PMMA-*g*-SF composite, the interfacial adhesion between the PMMA-grafted SF and PP is obviously improved, with the result that the PMMA-grafted SF was loaded to fracture [Fig. 10(c)]. This is because the presence of the PMMA layer covering the sisal fiber surface enhances the compatibility between SF and the PP matrix.

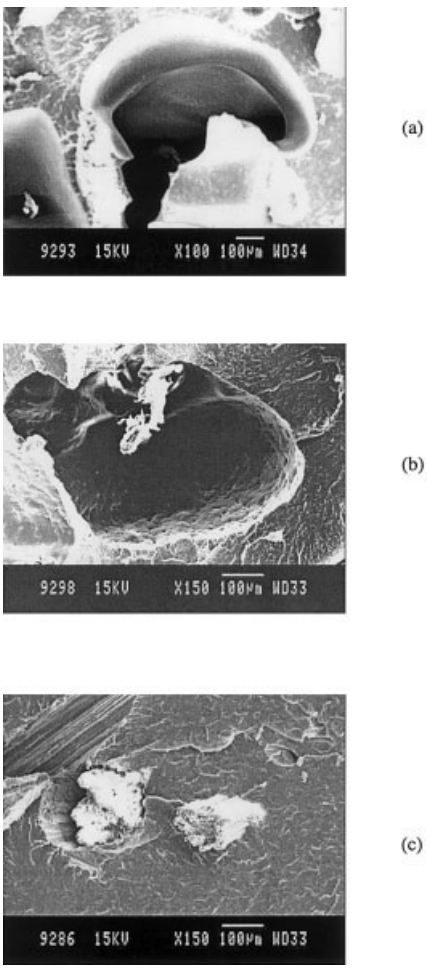

Figure 10 SEM micrographs of impact fracture samples: (a) PP/U-SF composite; (b) PP/AT-SF composite; (C) PP/PMMA-*g*-SF composites.

Crystal structure of PP/SF composites

The WAXD patterns of PP and the different PP/SF composites are displayed in Figure 11. PP possesses

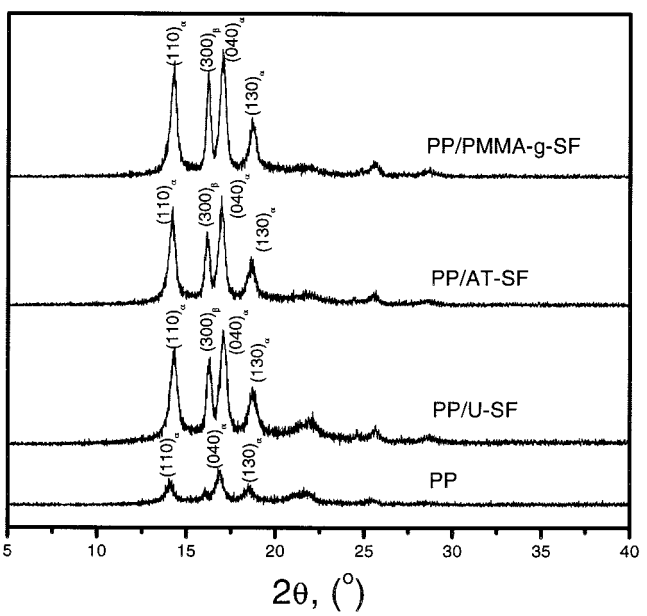

Figure 11 WAXD patterns of PP and the different PP/SF composites.

TABLE V
WAXD Data for PP and Different PP/SF Composites

Sample	Diffraction peak	2θ (°)	*d* (Å)	*I* (%)	L_{hkl} (Å)	*K* (%)
PP	$(110)_\alpha$	14.08	6.29	64	140.33	
	$(040)_\alpha$	16.87	5.25	100	146.62	
	$(130)_\alpha$	18.50	4.80	41	104.32	
PP/U-SF	$(110)_\alpha$	14.29	6.19	81.8	175.64	
	$(300)_\beta$	16.26	5.45	68.9	220.91	17.8
	$(040)_\alpha$	17.07	5.19	100	176.17	
	$(130)_\alpha$	18.68	4.75	38.7	117.90	
PP/AT-SF	$(110)_\alpha$	14.19	6.24	89.0	175.64	
	$(300)_\beta$	16.14	5.49	66.2	220.91	18.9
	$(040)_\alpha$	16.96	5.22	100	176.17	
	$(130)_\alpha$	18.64	4.76	37.2	126.24	
PP/PMMA-*g*-SF	$(110)_\alpha$	14.25	6.21	87.3	194.61	
	$(300)_\beta$	16.18	5.47	73.7	276.17	20.9
	$(040)_\alpha$	17.00	5.21	100	185.17	
	$(130)_\alpha$	18.68	4.74	39.2	159.98	

strong diffraction peaks at 14.08, 16.87, and 18.50°. These peaks correspond, respectively, to the (110), (040), and (130) diffraction planes of the α-form of PP crystals with a monoclinic configuration.[25] For the three PP/SF composites under investigation, an additional peak located at 16.2° is found in the WAXD spectrum. This peak is the characteristic (300) diffraction plane of the β-form of PP crystals with a hexagonal configuration. This indicates that the incorporation of SF induces the formation of the β-form of PP crystals in the PP/SF composites. The results are in accordance with our previous study.[9] The relative amount of the β-form of PP crystals (*K*-value) is determined by the following equation:

$$K = \frac{I_\beta}{(I_{\alpha 1} + I_{\alpha 2} + I_{\alpha 3} + I_\beta)} \quad (5)$$

where I_β, $I_{\alpha 1}$, $I_{\alpha 2}$, and $I_{\alpha 3}$ are intensities of (300), (110), (040), and (130) diffractions, respectively.

The interplanar spacing (*d*) values for the various peaks and the apparent crystal size (L_{hkl}) of PP in the direction perpendicular to the (*hkl*) crystal plane can be determined from Bragg's law and Scherrer's equation , respectively[26]:

$$d = \frac{\lambda}{2 \sin \theta} \quad (6)$$

$$L_{hkl} = \frac{k\lambda}{\beta_0 \cos \theta} \quad (7)$$

$$\beta_0 = \sqrt{\beta^2 - b_0^2} \quad (8)$$

where β_0 is the half-width of the reflection corrected for the instrumental broadening according to eq. (8); β is the half-width of the various diffraction peaks; b_0 is the instrumental broadening factor (0.15°); λ is the wavelength of the radiation used; and *k* is the instrument factor (0.9).

Table V summarizes the structural parameters determined from the WAXD curves. It can be seen that the incorporation of SF and surface treatment of SF have hardly any effect on the interplanar spacing *d*, but they have a significant influence on the apparent crystal sizes L_{hkl} corresponding to the several diffraction peaks. The $L_{(110)\alpha}$, $L_{(040)\alpha}$, $L_{(130)\alpha}$, and $L_{(300)\beta}$ of the α- and β-form PP crystals in the PP/SF composites increase considerably as SF is introduced into PP. Additionally, these values in the PP/PMMA-*g*-SF composites are higher than those in the PP/U-SF and PP/AT-SF composites. At the same time, the amount of β-form PP crystals (*K*-value) is maximum in the PP/PMMA-*g*-SF composites attributed to the better dispersion of SF in the PP matrix.

Mechanical properties of PP/SF composites

The tensile and impact properties of the three PP/SF composites are shown in Table VI. The Young's modulus, tensile strength, and Izod impact strength of the PP/PMMA-*g*-SF composite are all slightly higher than those of the PP/AT-SF and PP/U-SF composites.

As discussed in earlier sections, the alkali treatment removes the organic gum from the sisal fibers. This leads to an increase in the contacted area between SF and the PP matrix, and therefore improves the rein-

TABLE VI
Mechanical Properties of PP/SF Composites

Sample	Tensile strength (MPa)	Tensile modulus (GPa)	Izod impact strength (KJ/m^2)
PP/U-SF	27.6	1.55	6.70
PP/AT-SF	27.7	1.58	6.72
PP/PMMA-*g*-SF	28.6	1.67	7.40

forcement and toughening effects of SF to the PP matrix. For the PP/PMMA-*g*-SF composite, besides the removal of the organic gum, the SF surface–grafted PMMA induces better interfacial bonding between PP and SF. Furthermore, the enhanced fibrillation of the PMMA-grafted sisal fibers [see Fig. 5(b)] can also improve the stress transfer efficiency. The β-form of PP crystals is known to possess better impact strength than that of the α-form.[27] Because the amount of β-form PP crystals (*K*-value) in PP/PMMA-*g*-SF composites is higher than that in both the PP/AT-SF and PP/U-SF composites, this also contributes to the higher impact strength for the PP/PMMA-*g*-SF composite.

CONCLUSIONS

With the method adopted in this work, PMMA was successfully grafted onto sisal fiber surfaces. The sisal fiber surface–grafted PMMA enhances the interfacial adhesion between sisal fiber and the PP matrix. Addition of sisal fibers encouraged the formation of β-form PP crystals, with the PP/PMMA-*g*-SF composite possessing the highest *K*-value compared with that of either the PP/AT or the PP/U-SF composite. The higher *K*-value in the PP/PMMA-*g*-SF composite offers a better impact strength.

This work was supported by a grant from the Research Grants Council of the Hong Kong Special Administrative Region, China (Project No. 9040422).

References

1. Joseph, K.; Thomas, S.; Paul, A. Compos. Sci. Tech. 1997, 57, 67.
2. Joseph, K.; Thomas, S.; Pavithran, C. Polymer 1996, 37, 5139.
3. Joseph, P. V.; Joseph, K.; Thomas, S. Compos Sci Technol 1999, 59, 1625.
4. Prasad, S. V.; Pavithran, C.; Rohatgi, P. K. J Mater Sci 1983, 18, 1443.
5. Valadez-Gonzalez, A.; Cervantes-Uc, J. M.; Olayo, R.; Herrera-Franco, P. J. Composites Part B 1999, 30, 309.
6. Bledzki, A. K.; Gassan, J. Prog Polym Sci 1999, 24, 221.
7. Saheb, D. N.; Jog, J. P. Adv Polym Technol 1999, 18, 351.
8. Li, Y.; Mai, Y.-W.; Ye, L. Compos Sci Technol 2000, 60, 2037.
9. Xie, X. L.; Li, R. K. Y.; Tjong, S. C.; Mai, Y.-W. Polym Compos 2002, 23, 319.
10. Bisanda, E. T.; Ansell, M. P. Compos Sci Technol 1991, 41, 165.
11. Joseph, K.; Varghese, S.; Kalaprasad, G.; Thomas, S.; Prasannakumari, L.; Koshy, P.; Pavithran, C. Eur Polym J 1996, 32, 1243.
12. Bai, S. L.; Li, R. K. Y.; Wu, L. C. M.; Zeng, H. M.; Mai, Y.-W. J Mater Sci Lett 1998, 17, 1805.
13. Bai, S. L.; Wu, C. M. L.; Mai, Y.-W.; Zeng, H. M.; Li, R. K. Y. Adv Compos Lett 1999, 8, 13.
14. Tsang, F. F. Y.; Jin, Y. Z.; Yu, K. N.; Wu, C. M. L.; Li, R. K. Y. J Mater Sci Lett 2000, 19, 1155.
15. Xie, X. L.; Fung, K. L.; Li, R. K. Y.; Tjong, S. C.; Mai, Y.-W. J Polym Sci Part B: Polym Phys 2002, 40, 1214.
16. Singh, B.; Gupta, M.; Verma, A.; Tyagi, O. Polym Int 2000, 49, 1444.
17. Ichazo, M. N.; Albano, C.; Gonzalez, J. Polym Int 2000, 49, 1409.
18. Xie, X. L.; Li, B. G.; Pan, Z. R.; Li, R. K. Y.; Tjong, S. C. J Appl Polym Sci 2001, 80, 2105.
19. Canché-Escamilla, G.; Rodríguez-Trujillo, G.; Herrera-Franco, P. J.; Mendizábal, E.; Puig, J. E. J Appl Polym Sci 1997, 66, 339.
20. Canché-Escamilla, G.; Cauich-Cupul, J. I.; Mendizábal, E.; Puig, J. E.; Vázquez-Torres, H.; Herrera-Franco, P. J. Composites Part A 1999, 30, 349.
21. Van Krevelen, D. W. Properties of Polymers, 3rd rev. ed.; Elsevier Scientific: Amsterdam/New York, 1997.
22. McCrum, N. G.; Read, B. E.; Willians, G. Anelastic and Dielectric Effects in Polymeric Solids; Dover: New York, 1967.
23. Díez-Gutiérrez, S.; Rodríguez-Pérez, M. A.; De Saja, J. A.; Velasco, J. I. Polymer 1999, 40, 5345.
24. Murayama, T. Dynamic Mechanical Analysis of Polymeric Material; Elsevier Scientific: Amsterdam/New York, 1978.
25. Karger-Kocsis, J. Polypropylene: Structure, Blends and Composites; Chapman & Hall: London/New York, 1995.
26. Alexander, L. E. X-Ray Diffraction Methods in Polymer Science; Wiley-Interscience: New York, 1969.
27. Tjong, S. C.; Shen, J. S.; Li, R. K. Y. Polym Eng Sci 1996, 36, 100.